Hindawi
Geofluids
Volume 2020, Article ID 8812188, 19 pages
https://doi.org/10.1155/2020/8812188

Research Article

Mechanical Behavior Evolution and Damage Characterization of Coal under Different Cyclic Engineering Loading

Huajun Wang and Jian Li

School of Mines and Civil Engineering, Liupanshui Normal University, Guizhou 553004, China

Correspondence should be addressed to Huajun Wang; 248300579@qq.com

Received 25 July 2020; Accepted 16 September 2020; Published 5 October 2020

Academic Editor: Zhijie Wen

The cyclic loading causes the strength change of porous rocks, which can be frequently encountered in underground coal mining. In order to quantify the cumulative damage of porous coal, multilevel uniaxial cyclic compressive tests were carried out considering different loading frequencies. The results show that under cyclic loading, Young's modulus of coal shows a first drastic increase and then decrease trend in terms of the number of loading-unloading cycles, while the Poisson's ratio gradually increased at lower peak stress amplitudes and then increased sharply with peak cyclic stress amplitude until losing load bearing capacity, following a stepwise rising trend. At a higher loading frequency, volumetric compressibility-dilatancy transition is shifted to an earlier time. The loading/unloading response ratio (LURR) was used to evaluate the damage of coal under cyclic loading. It is found that LURR is an effective parameter to evaluate the damage of coaly rock under cyclic loading and is also useful in distinguishing different deformation mechanism at different loading stages. The results also show that the damage of coal can initiate at the early stage of cyclic loading at a low loading frequency; however, the increase in frequency of cyclic loading can delay the damage time, requiring a relatively higher level of peak cyclic stress amplitude.

1. Introduction

Ground control has been deemed as one of most important issues in many rock engineering applications, and its prerequisite is to evaluate and characterize the geotechnical property evolution of porous rocks, such as coal and shale [1, 2]. Different from monotonic load, cyclic loading is time dependent in a repeated manner and usually expressed by superposition of a mean stress σ_{mean} and a periodically time-dependent cyclic amplitude $\Delta\sigma$ in mathematics [3]. The cyclic loading at different loading rates and frequencies can degrade the strength properties of rocks [4–7]. Thus, it is unfavorable to the stability of rock structures in underground coal mining. In underground mining, the cyclic loading can be induced by the back-and-forth coal cutting, periodic overlying roof strata weighting, drilling, and blasting. Furthermore, the coal contains a wide pore-size distribution, cleat, and butt systems, making its mechanical behavior more complex than that of salt rock, granite, sandstone, and limestone [8–11]. Therefore, quantification of coal damage under cyclic loading, especially in the early stages of microcrack initiation and propagation, is important for a proper understanding of its cyclic behavior [12].

Cyclic loading often causes rock to fail at a lower stress amplitude than its uniaxial compressive strength. A slight degradation in mechanical properties of rocks is mainly induced by fatigue damage under cyclic loading. To date, many studies have been made to the mechanical properties and deformable behaviors of rocks under uniaxial cyclic loading [13–15]. Different from the uniaxial cyclic loading tests, the confining pressure can improve fatigue strength of rock. The mechanical properties and deformable behaviors of rocks under triaxial cyclic loading had also investigated [16–18]. Overall, the triaxial compressive strength and total strain of rocks increased with the enhancement of confining pressure under cyclic loading. The triaxial strength of sandstone under cyclic loading can sometimes be higher than that of monotonic loading at lower confining pressure [19]. But the triaxial strength of sandstone is approximately equal to that of monotonic loading at a higher confining pressure.

(a) (b)

Figure 1: Photographs of coal samples: (a) uniaxial compressive tests; (b) cyclic loading tests.

In addition, the fatigue life of rocks has been investigated, which shows that the fatigue life of rocks increased with the increase of loading frequency and decreased with the increase of stress amplitude [20, 21]. Although the mechanical properties and deformation behavior of rocks have been investigated under multilevel cyclic loading tests, the complete understanding has not been achieved. Also, the loading rate kept constant during the whole cyclic loading tests in most existing studies. Furthermore, due to the pore structure complexity and heterogeneity caused by the coalification process, the fatigue characteristics of coal with an increasing loading rate need to be further studied, especially the influence of peak cyclic stress amplitude and loading frequency on damage evolution of coal.

To quantify the damage evolution of rocks, the fatigue damage model of rocks defined by different variables had been extensively studied, including the irreversible strain [22–24], an isothermal creep model [25], dissipated energy theory [26], linear accumulation method [27], and an empirical model [28]. Generally, these damage models are competent to describe the whole fatigue damage of rocks under cyclic loading. But the previous literature mainly focuses on nonorganic rocks, rather than coal. Also, the organic coal is complex in pore structure by containing a wider distribution in pore size, cleat, and butt system, which may make it different from laboratory-scale intact granite, siltstone, sandstone, and rock salt on the micro scale when subjected to repetitive loading and unloading.

In this study, multilevel uniaxial cyclic compressive tests were carried out on coal under different peak stress amplitudes and frequencies. Then, the mechanical properties and deformation behavior of coal were analyzed. The dissipated energy and AE characteristics of coal were further discussed in details. At last, the fatigue damage evolution of coal was quantitatively analyzed based on load-unload response ratio theory and cumulative damage model.

2. Material and Methods

2.1. Sample Preparation and Description. The fresh coal blocks were collected from Gaojialiang Mine, Inner Mongolia, China. After sealing with membrane wrap, large blocks of coal were then transported to the laboratory, and the coal samples were cored with the drilling rig to be 50 mm in diameter. Finally, the cylindrical samples were trimmed and the two ends of each sample were polished with the lapping machine to be a height to diameter ratio of 2 : 1 [29] A total of 15 coal samples were initially prepared. However, coal is typically soft organic sedimentary rock, fragile to core drilling, and two-parallel-end polishing. Also, great heterogeneity exists in coal sampling. These can induce large scatter in testing results. In order to reduce such scatter, sonic tests were conducted for initial sample identification and only coal samples of similar wave velocity were selected in this study. Finally, 7 coal specimens were used for the compressive tests, in which coals samples, C1, C2, and C3, were selected to measure the uniaxial compressive strength (*UCS*), while coal samples, C7, C8, C9, and C10, were used for cyclic loading tests. Figure 1 presents the photographs of coal samples before experiment.

The coal samples have an average density of 1.46 g/cm^3 and porosity of 7.93%. In order to have a proper understanding of the mechanical property of coal samples, the uniaxial monotonic compressive tests (*UCS*) were conducted to measure its mechanical properties. Three coal samples were tested at the loading rate of 0.1 mm/min using the MTS 815 servo-hydraulic testing system. The average uniaxial compressive strength of coal was 16.8 MPa. The average Young's modulus of coal was 2.73 GPa, while the average Poisson's ratio of coal was 0.217. Figure 2 shows the conventional monotonic testing results for coal samples C1, C2, and C3.

2.2. Test Set-Up and Procedure. The MTS 815 servo-hydraulic testing system was used for *UCS* and cyclic loading tests. The MTS testing system mainly consists of a compressive loading frame, an axial loading system, and a data acquisition system. It can provide a closed-loop servo-hydraulic control in material testing. The testing frame has a compressive loading capacity of 2,600 kN.

Prior to cyclic tests, the monotonic compression was conducted to obtain the basic mechanical properties of coal. The measured *UCS* of coal is taken as the reference loading for the peak loading amplitude of cyclic tests. The increasing multilevel cyclic loading tests were performed using axial control with a sinusoidal wave, and the loading frequency was set to be 0.1 Hz, 0.2 Hz, and 0.5 Hz, respectively. The peak stress amplitudes are set as 20%, 40%, 60%, and 80% of the *UCS* of coal. The lower bound of stress amplitude was 5% of *UCS*. Each stress level was repeated twenty times. During the tests, extensometers of model 632.9X were used to measure the

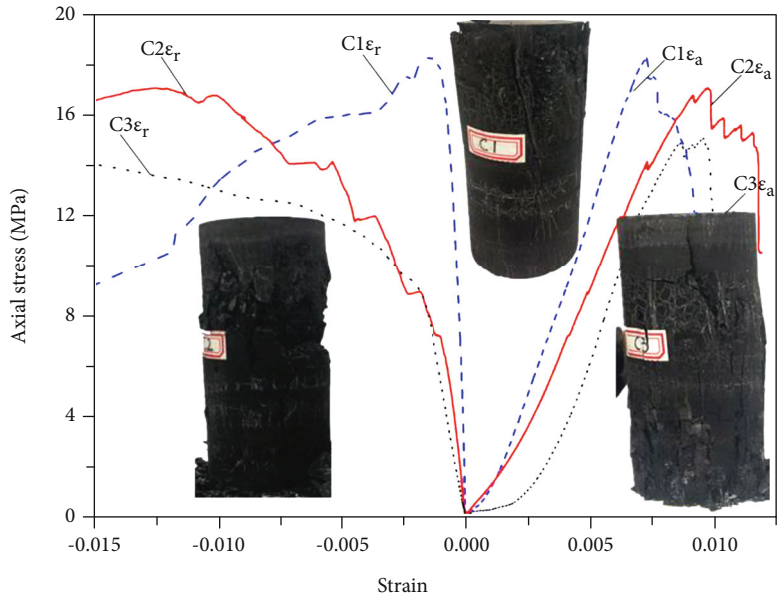

Figure 2: Stress-strain curves of coal in uniaxial compressive tests.

axial and radial strain of coal samples. Experimental data were recorded by every 0.1 s. Meanwhile, the PCI-2 acoustic emission (AE) system, American Physical Acoustics Company, was used to simultaneously capture the AE characteristics. The preamplifier and threshold value of AE system were set to 40 dB and 38 dB, respectively. The MTS 815 testing system and AE system are illustrated in Figure 3.

3. Results and Discussion

3.1. Stress-Strain Curves. Figure 4 shows the stress-strain curves of coal under multilevel cyclic loading frequencies from 0.1 Hz to 0.5 Hz. Overall, the rate of deformation accumulation was not constant at the same peak stress amplitude, irrespectively of the loading frequency. The increment of axial strain of the first loading and unloading cycle is highest over the rest of subsequent individual cycles. In other words, a relatively larger amount of irreversible deformation occurred in the first cyclic loading. After that, the induced damage of coal by individual cyclic loading cycle is smaller. This is the rock damage difference between monotonic loading and cyclic loading.

Figure 4 also shows the hysteresis loops were mostly straight and closed at lower peak stress amplitudes, implying that the produced plastic deformation was small. However, the hysteresis loops became loose at the higher stress amplitudes, indicating that the plastic deformation gradually increased with the increase of stress amplitude.

At the loading frequency of 0.5 Hz, the fatigue failure of coal sample occurred at the cycle number of 74, but no macro failure occurred for coal samples under loading frequency of 0.1 Hz and 0.2 Hz. In addition, the opening-closing-opening pattern of radial strain was observed at the loading frequency of 0.5 Hz. Such phenomenon was also observed in the marble [30]. The first opening-up of radial strain was due to the energy dissipation contributed to crack growth. Owing to

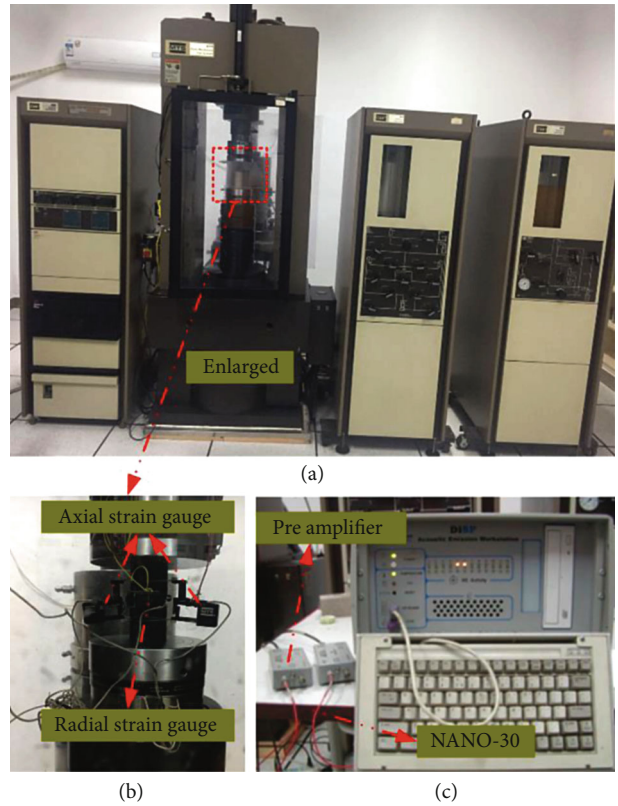

Figure 3: Diagram of the experimental system: (a) MTS 815 test system; (b) external measuring device; (c) AE device.

the frictional resistance by grain contact, the closing occurred in the following cyclic loading. The crack growth became dominant again when the coal approached to the limit of macro failure. In order to exclude the impact of coal sample heterogeneity, extra cyclic loading tests were conducted at the loading frequency of 0.5 Hz, and the coal samples failed

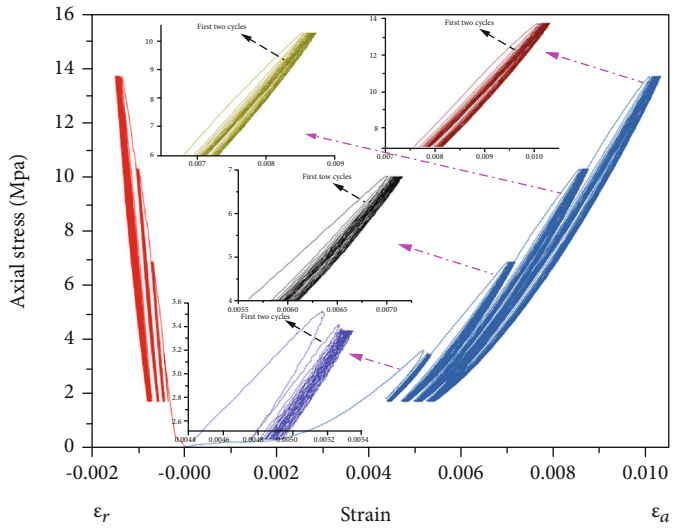

(a)

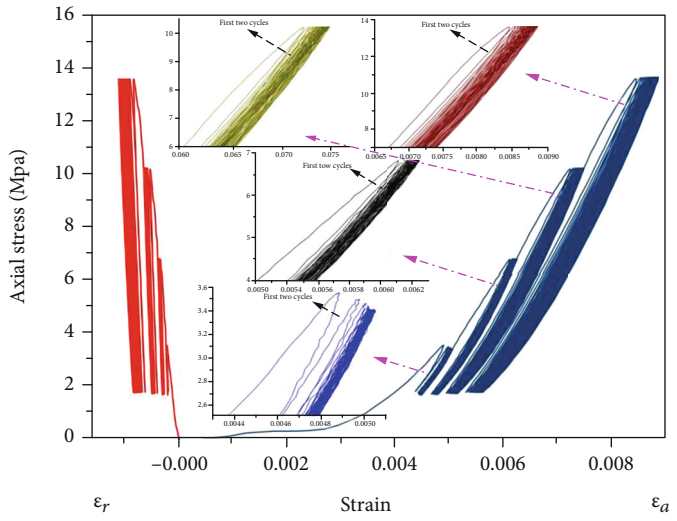

(b)

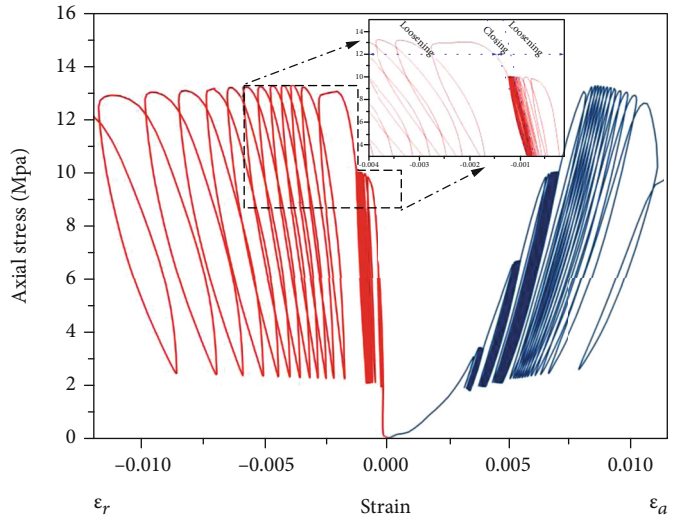

(c)

Figure 4: Stress-strain curves of coal with multilevel stress at different loading frequencies: (a) 0.1 Hz; (b) 0.2 Hz; (c) 0.5 Hz.

in the same manner. Therefore, the higher loading frequency and stress amplitude lead to greater damage, thus shortening fatigue life of coal.

3.2. Mechanical Property and Deformability Evolution

3.2.1. Evolution of Young's Modulus. In cyclic behavior analysis, the average slope of the straight line portion of the axial stress-strain curve is taken as the tangent Young's modulus E [28]. During each cyclic loading and unloading tests, the tangent Young's modulus and Poisson's ratio are defined as follows:

$$E = \frac{\Delta\sigma_{\mathrm{a}}}{\Delta\varepsilon_a}, \tag{1}$$

$$\mu = -\frac{(\Delta\sigma_a/\Delta\varepsilon_a)}{(\Delta\sigma_a/\Delta\varepsilon_r)}, \tag{2}$$

where $\Delta\sigma_a$ is the increment of axial stress, the $\Delta\varepsilon_a$ is the increment of axial strain, and $\Delta\varepsilon_r$ is the increment of radial strain.

Figure 5 shows the relationship between the Young's modulus and the number of cycles under different loading frequencies. In general, the Young's modulus increased gradually with the increase of peak stress amplitude under the same loading frequency, following a stepwise rising trend. Additionally, the Young's modulus initially showed a sharp increase in the first few cycles and kept almost invariable in the rest of loading cycles at a specific peak stress amplitude. Figure 5 also shows that the increment in Young's modulus is largest at the lowest peak stress amplitude, and the absolute increment gradually decreased with the increase of stress amplitude. This is attributed to the closure of microcracks and voids in the coal. At the first and lowest peak stress amplitude, many microcracks and voids within coal samples were compacted by cyclic loading, thus making the coal stiffer against deformation. With further continual of cyclic loading, including the increase in peak stress amplitude, the amount of compaction is smaller than that of the first lowest peak stress amplitude, as the deformation modulus of coal already increased by cyclic loading of previously lower peak stress amplitude, resulting in a small level of increase in Young's modulus. Under the loading frequency of 0.1 Hz, the average Young's modulus at peak stress amplitude of $0.2\sigma_c$, $0.4\sigma_c$, $0.6\sigma_c$, and $0.8\sigma_c$ is 1.92 GPa, 2.23 GPa, 2.39 GPa, and 2.49 GPa, respectively. With the peak stress amplitude increased gradually from $0.2\sigma_c$ to $0.8\sigma_c$, the average Young's modulus increased by 15.71%, 7.72%, and 3.92%, respectively. This decreasing trend in E of coal in terms of peak stress amplitudes is similar to the granite [18]. At the loading frequency of 0.2 Hz, the average Young's modulus corresponding to the abovementioned four peak stress amplitude is 2.86 GPa, 3.44 GPa, 3.65 GPa, and 3.70 GPa. When the cyclic loading increased from the $0.2\sigma_c$ to the final $0.8\sigma_c$, the average Young's modulus increased by 20.21%, 6.04%, and 1.45%, respectively. For the loading frequency of 0.5 Hz, the coal sample finally lost the bearing capacity by developing obliquely macro fracture when the cyclic loading entered into the fourth stress level. It is also noticed that more debris produced from the failed coal sample when compared to *UCS* tests. As the peak stress amplitude increased from the $0.2\sigma_c$ to $0.6\sigma_c$, the average Young's modulus increased by 22.51% and 3.35%, respectively. Figure 5 also shows that there is a decreasing trend in E with the increase of loading frequency, even though the coal specimens are different. Therefore, the frequency of cyclic loading has a significant influence on the mechanical property and fatigue life of coal.

3.2.2. Evolution of Poisson's Ratio. The evolution of Poisson's ratio under multilevel cyclic loading at different frequencies is plotted in Figure 6. Different from the variation trend of Young's modulus, the Poisson's ratio displayed a first reduction and then a relatively stable trend under the cyclic loading of the first peak stress amplitude. Such a decrease in Poisson's ratio is due to closure of initial microcracks or pores in the coal. This phenomenon can also be verified in Figure 5. After the first peak stress amplitude, the Poisson's ratio increased in the first loading cycle and then maintained almost invariable in the rest of 19 loading cycles for the peak stress amplitude of $0.4\sigma_c$ and $0.6\sigma_c$. The increase in Poisson's ratio is due to the initiation of new microcracks or the growth of existing microcracks. For the peak stress amplitude of $0.8\sigma_c$, the evolution rate of Poisson's ratio increased gradually with respect to the cycles at the loading frequency of 0.1 Hz and 0.2 Hz. Due to the failure of coal sample in the end, a sharply increasing rate of Poisson's ratio was observed at the loading frequency of 0.5 Hz.

Figure 6 shows that for the loading frequency of 0.1 Hz, the average Poisson's ratio increased by 7.99%, 12.77%, and 14.28% when the peak stress amplitude of cyclic loading increased from $0.2\sigma_c$ to $0.8\sigma_c$. For the loading frequency of 0.2 Hz, the increment of average Poisson's ratio was 8.62%, 15.81%, and 25.01% when the cyclic loading increased from $0.2\sigma_c$ to $0.8\sigma_c$. For the loading frequency of 0.5 Hz, the average Poisson's ratio was 0.057, 0.104, 0.183, and 0.637 when the stress levels increased from the first to the fourth. The increment of Poisson's ratio was 82.46%, 75.96%, and 248.09%, respectively.

3.2.3. Evolution of Irreversible Axial and Radial Strains. Figure 7 shows the evolution of irreversible axial and radial strain with respect to the number of cycles at different loading frequencies. The evolution of the irreversible axial and radial strains is similar under different loading frequency. A slight change in axial and radial irreversible strains was observed at the first level of peak stress amplitude. After that, the irreversible strain gradually increased with the increase of stress level. Therefore, the fatigue damage gradually developed with the increase of stress amplitude and cycle numbers. Different from the loading frequency of 0.1 Hz and 0.2 Hz, the variation of irreversible axial and radial strains at the loading frequency of 0.5 Hz exhibited a typical three-phase trend in terms of the peak stress amplitude level. In the first phase which corresponded to the first stress level, both the axial and radial residual strains approximately remained constant. In the second phase corresponding to

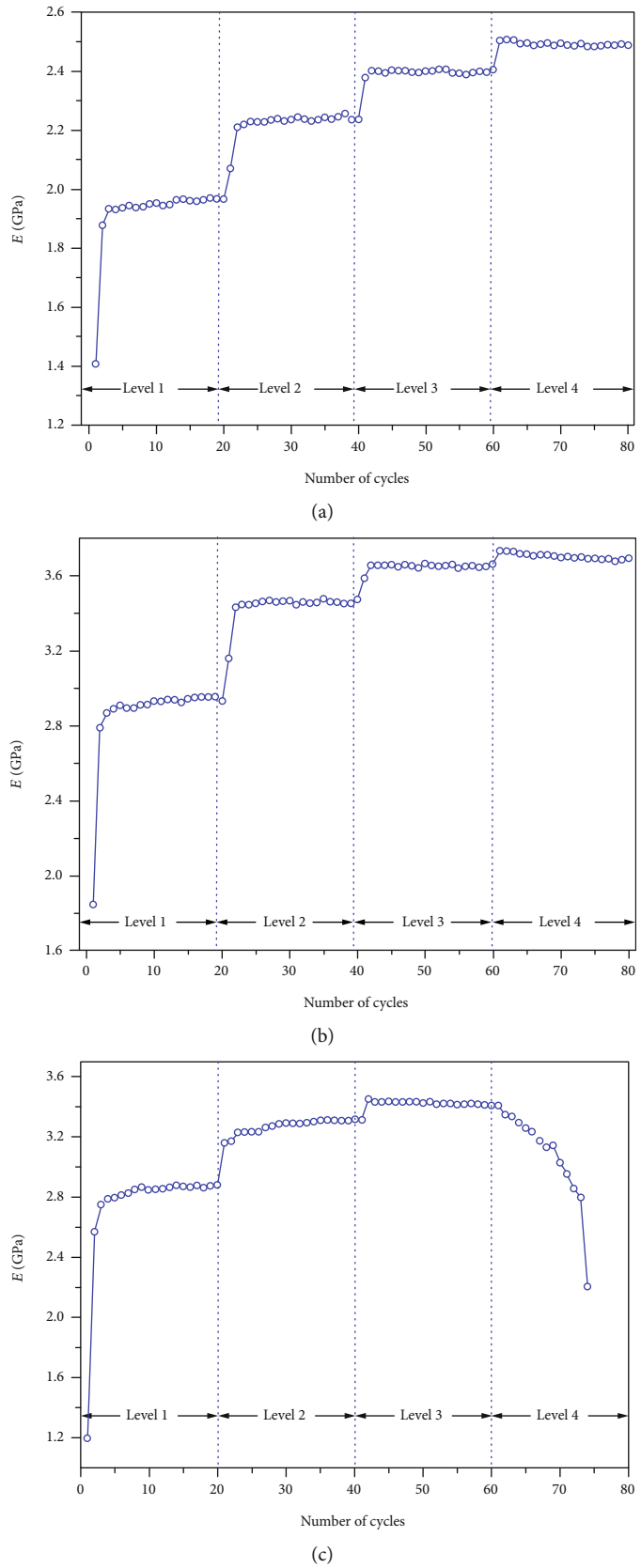

Figure 5: Evolution of Young's modulus with the number of cycles under different frequencies: (a) 0.1 Hz; (b) 0.2 Hz; (c) 0.5 Hz.

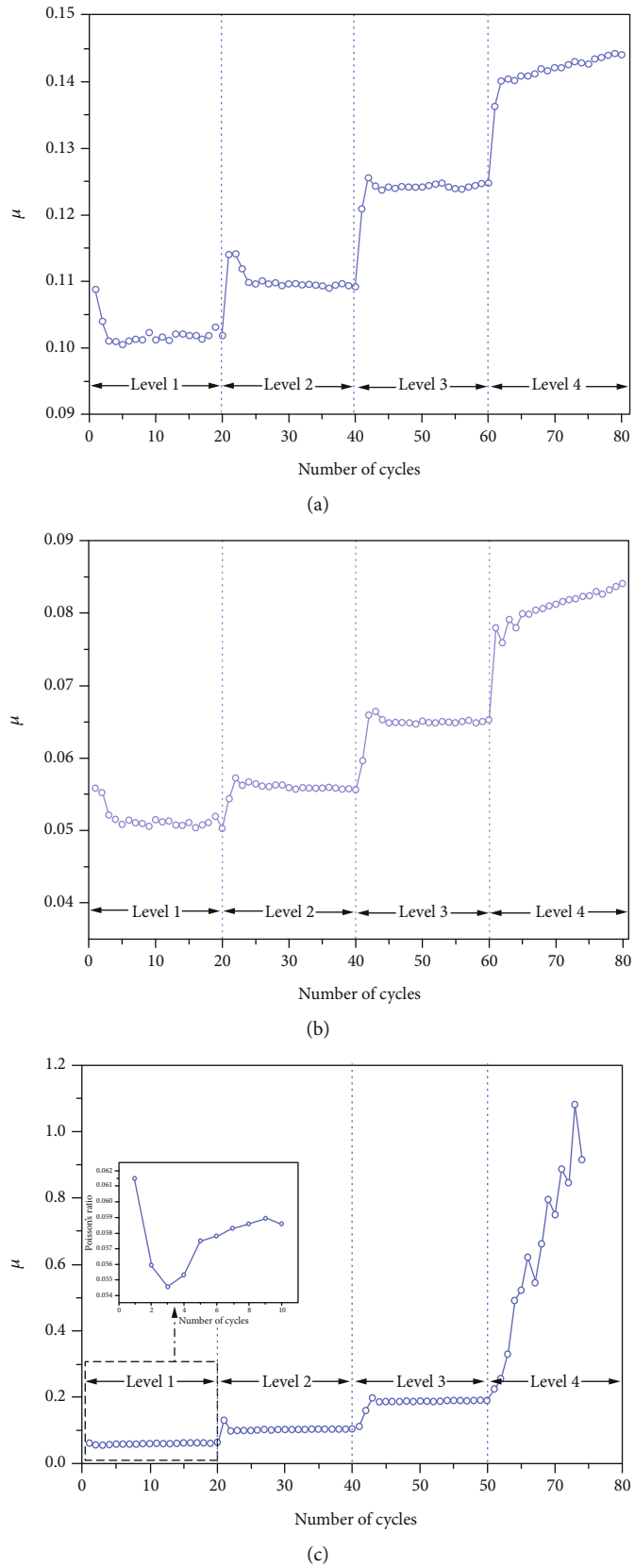

Figure 6: Evolution of Poisson's ratio with the number of cycles under different frequencies: (a) 0.1 Hz; (b) 0.2 Hz; (c) 0.5 Hz.

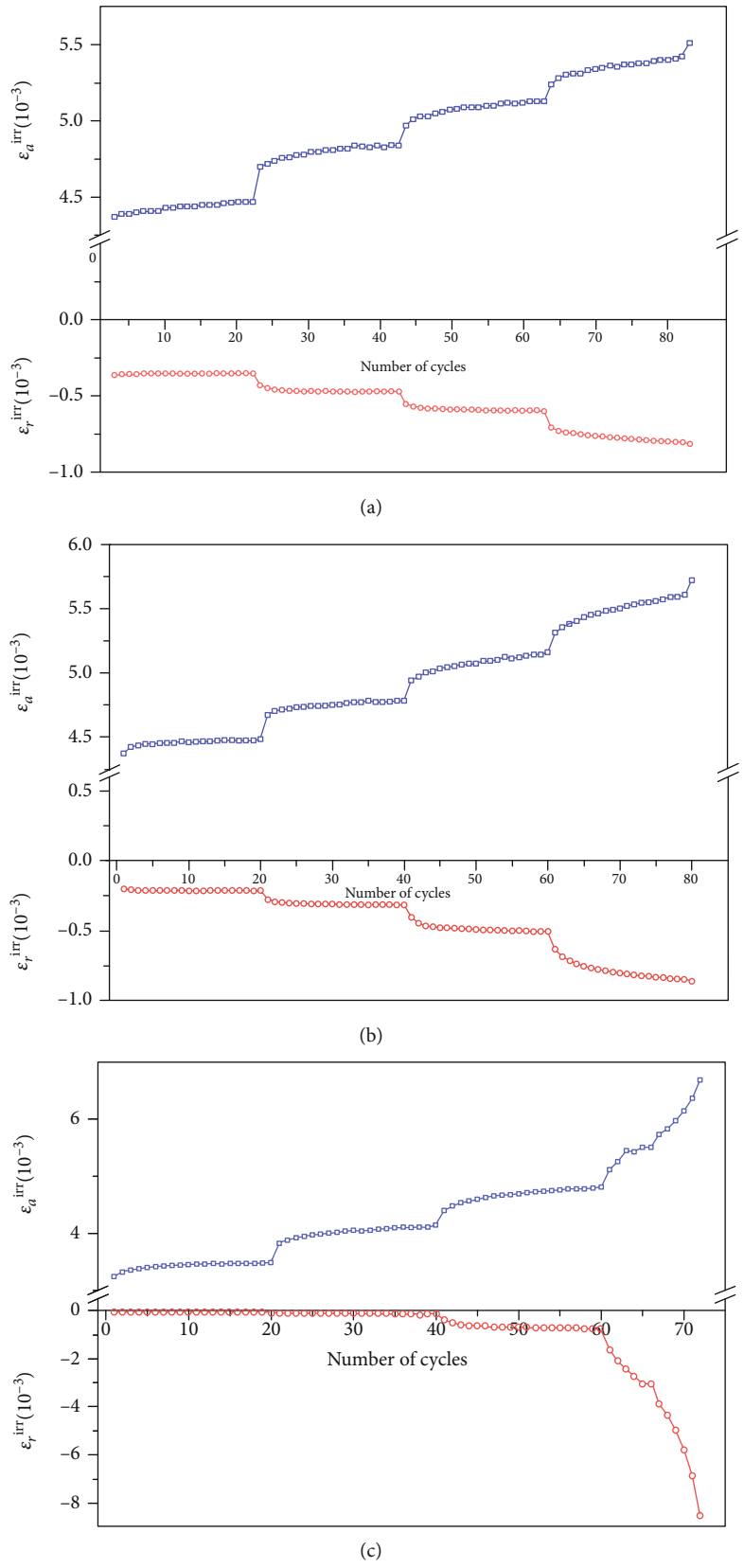

Figure 7: Evolution of irreversible strain with the number of cycles under different loading frequencies: (a) 0.1 Hz; (b) 0.2 Hz; (c) 0.5 Hz.

the second and third stress levels, the residual strain increased gradually with respect to the cycles. In the third phase corresponding to the acceleration phase, both the axial and radial residual strains increased sharply with the number of cycles.

3.2.4. Evolution of Irreversible Volumetric Strain. Figure 8 shows the evolution of irreversible volumetric strain with the number of cycles under different loading frequencies. The variation of the irreversible volumetric strain is nonmonotonic. For the loading frequency of both 0.1 Hz and 0.2 Hz, compressibility-dilatancy transition occurred in the peak stress amplitude level of $0.8\sigma_{c.}$ The irreversible volumetric strain showed an overall increased trend in first three peak stress amplitude levels at the loading frequencies of 0.1 Hz and 0.2 Hz, even though fluctuation exists. In this phase, the compaction of primary microcracks or voids in coal dominated in deformation. After that, the volumetric strain decreased significantly at the fourth peak stress amplitude level of $0.8\sigma_c$, where the dilatancy of coal sample occurred. On the micro scale, the new microcracks were developed in coal sample at this stress level. Different from the loading frequency of 0.1 Hz and 0.2 Hz, the deformation behavior of coal has changed from compaction to dilatancy at the loading frequency of 0.5 Hz (Figure 8(c)). Meanwhile, the dilatancy of coal initiated as early as the three peak stress amplitude levels. The macroscopic cracking of coal formed within the sample when the loading frequency entered into the fourth stress level, leading to the macro failure of coal sample.

3.3. Energy Characteristics of Coal Subjected to Multilevel Cyclic Loading under Different Frequencies. The deformation and failure of rock, including coal, is a progressive process of energy accumulation and release [31]. Energy analysis is conducted to characterize the fatigue damage of coal during the cyclic loading and unloading. The total strain energy U_t is developed due to external work. A part of strain energy is accumulated in the rock in the form of elastic deformation, namely, elastic energy U_e. The rest of strain energy U_d is released in the form of irreversible deformation, such as the development of cracks and internal frictional slip among grains. During the multilevel cyclic loading and unloading, the total strain energy, elastic energy, and the dissipated strain energy can be given as

$$U_t^i = AH\int \sigma_1 \mathrm{d}\varepsilon_1 = \sum_{i=1}^{n} \frac{1}{2}(\sigma_{1i} + \sigma_{1i-1})(\varepsilon_{1i} - \varepsilon_{1i-1}), \quad (3)$$

$$U_e^i = AH\int \sigma_2 \mathrm{d}\varepsilon_2 = \sum_{i=1}^{n} \frac{1}{2}(\sigma_{2i} + \sigma_{2i-1})(\varepsilon_{2i} - \varepsilon_{2i-1}), \quad (4)$$

$$U_d^i = U_t^i - U_e^i, \quad (5)$$

where U_t^i is the total strain energy during the process of ith loading phase, U_e^i is the elastic strain energy during the process of ith unloading phase, U_d^i is the dissipated strain energy corresponding to ith, A is the loading area of coal sample, H is the sample height, σ_1 and ε_1 are the axial stress and strain during the loading stage, and σ_2 and ε_2 are the axial stress and strain during the unloading stage.

The dissipated strain energy of coal at different loading frequencies is calculated based on Eqs. (3)–(5). Figure 9 shows the dissipated energy density of coal with the multilevel cyclic loading-unloading. Overall, the dissipated energy of coal increased with the increase of peak stress amplitude, even though a first decrease and then almost invariable trend of dissipated energy occurred under cyclic loading of each peak stress amplitude. In addition, the maximum dissipated energy density of coal occurred in the first cyclic loading at each peak stress amplitude level. This is due to the closure of existing microcracks and voids of coal, leading to the dissipated energy in coal increased rapidly in the first cyclic loading. Also, the largest dissipated energy density of coal increased gradually with the increase of stress amplitude.

For the loading frequency of 0.1 Hz, the average dissipated energy density was 130.5 J/m^3, 551.5 J/m^3, 1313.5 J/m^3, and 2393.0 J/m^3, respectively, by increasing 323.61%, 138.18%, and 82.19% at the peak stress amplitude of $0.2\sigma_c$, $0.4\sigma_c$, $0.6\sigma_c$, and $0.8\sigma_c$. For the loading frequency of 0.2 Hz, the increment of dissipated energy density also presented a gradual reduction trend with regard to the number cycles. When the cyclic loading increased from the first stress level ($0.2\sigma_c$) to the fourth ($0.8\sigma_c$), the average dissipated energy density of coal was 100.5 J/m^3, 337.5 J/m^3, 847.5 J/m^3, and 1776 J/m^3, respectively. The average dissipated energy density of coal increased by 235.82%, 151.11%, and 109.56%, respectively. Therefore, the increment of average dissipated energy density decreased with the increase in peak stress amplitude at the loading frequency of both 0.1 Hz and 0.2 Hz. However, different from the loading frequency of 0.1 Hz and 0.2 Hz, the increment of dissipated energy density tended to be a first decrease and then increased trend with respect to the number of cycles at the loading frequency of 0.5 Hz, where the increment of average dissipated energy density was 304.71%, 154.16%, and 242.86% when the peak stress amplitude increased from $0.2\sigma_c$ to $0.8\sigma_c$. Figure 9(b) shows the cumulative dissipated energy density of coal with regard to the number of cycles, where the cumulative dissipated energy density of coal increased exponentially with the increase of number of cycles. According to the characteristics of cumulative dissipated energy density of coal, the whole cyclic loading process of coal can be divided into three phases. The phase I corresponds to the first stress level and can be named as the initial phase. In this phase, the rate of cumulative dissipated energy of coal illustrated a slight increase trend with regard to the number of cycles. This is due to the closure of existing microcracks and voids of coal. Phase II corresponds to the second and third stress level, which can be termed as the steady phase. In this phase, the rate of cumulative dissipated energy of coal presented a gradual increase trend. Phase III corresponds to the fourth stress level ($0.8\sigma_c$), which can be referred as the accelerating phase. In this phase, the rate of cumulative dissipated energy increased sharply with the increase of cycles. In addition, the cumulative dissipated energy density of coal firstly decreased and then increased with the increase of cyclic loading frequency.

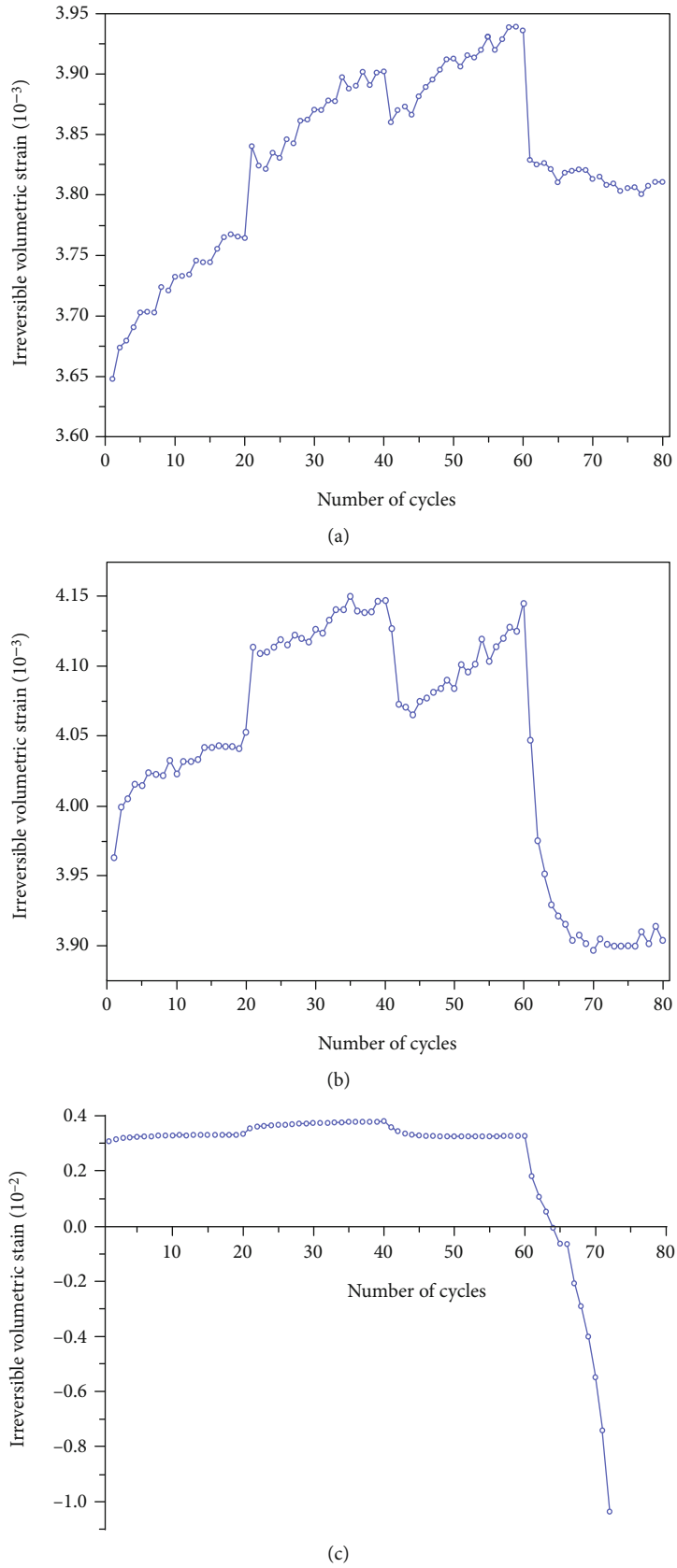

Figure 8: Evolution of irreversible volumetric strain with the number of cycles: (a) 0.1 Hz; (b) 0.2 Hz; (c) 0.5 Hz.

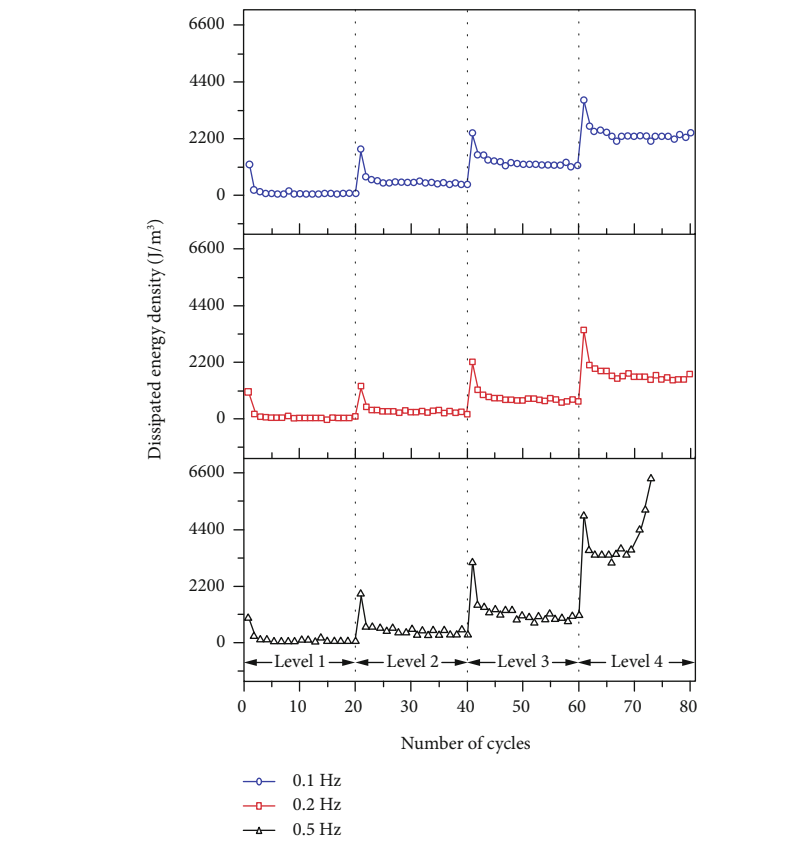

(a)

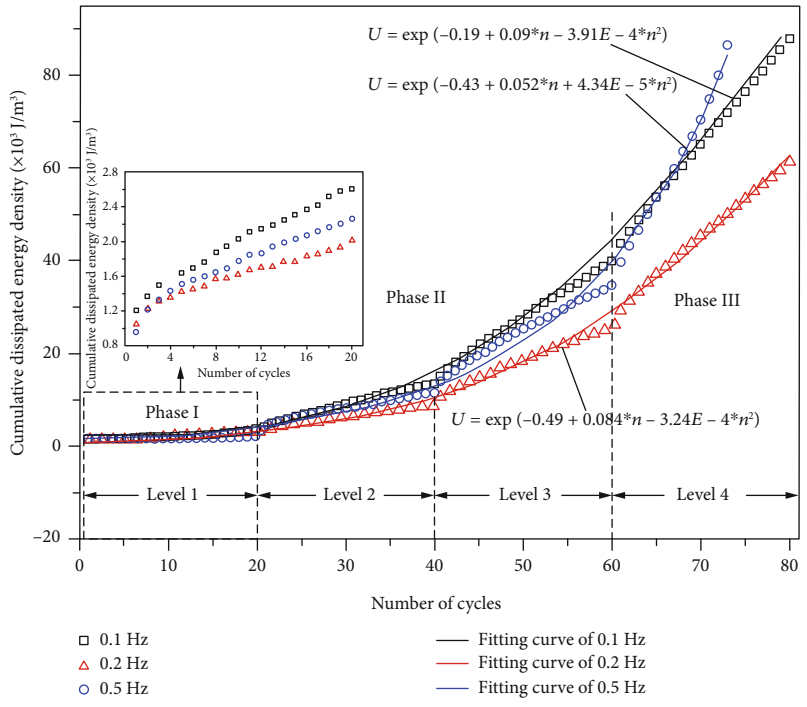

(b)

Figure 9: Evolution of dissipated energy of coal versus cycles at different loading frequencies: a dissipated energy; b cumulative dissipated energy density.

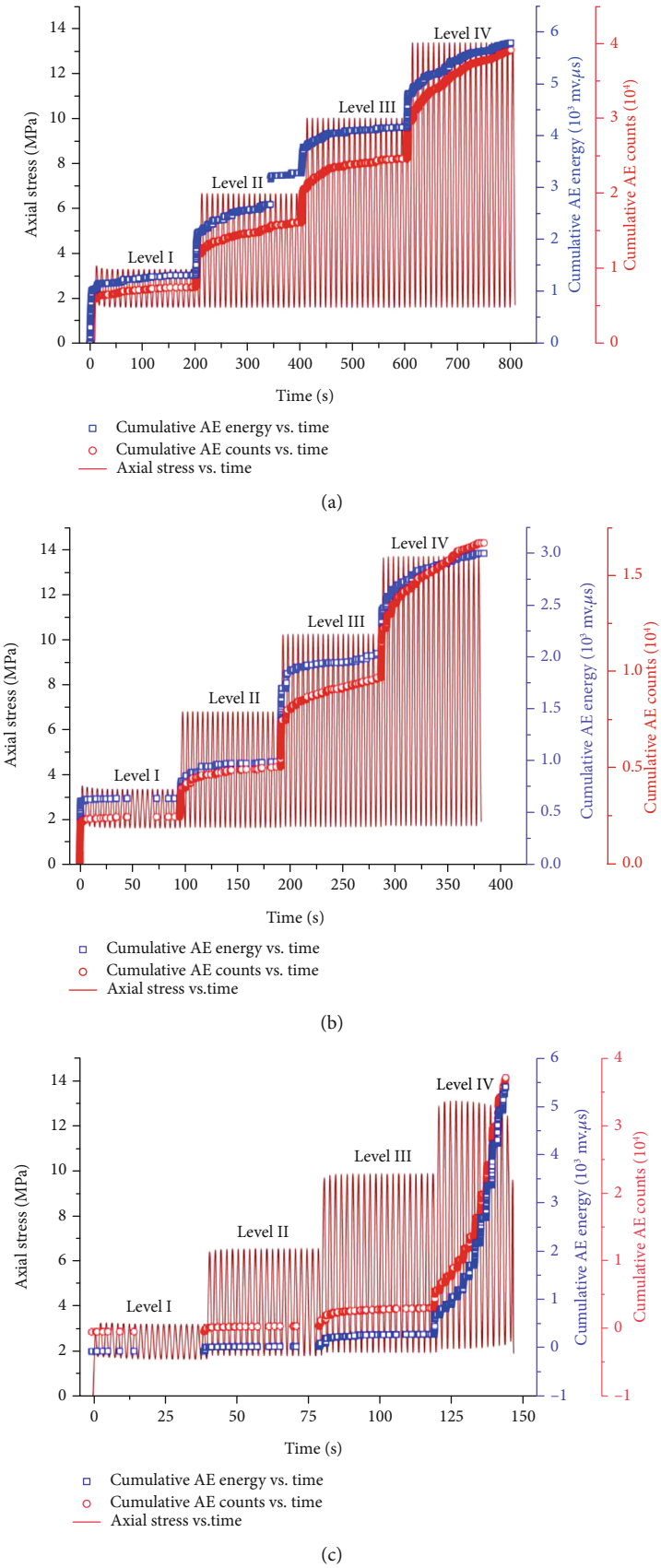

Figure 10: Evolution of axial stress and AE events of coal versus time at different loading frequencies: (a) 0.1 Hz; (b) 0.2 Hz; (c) 0.5 Hz.

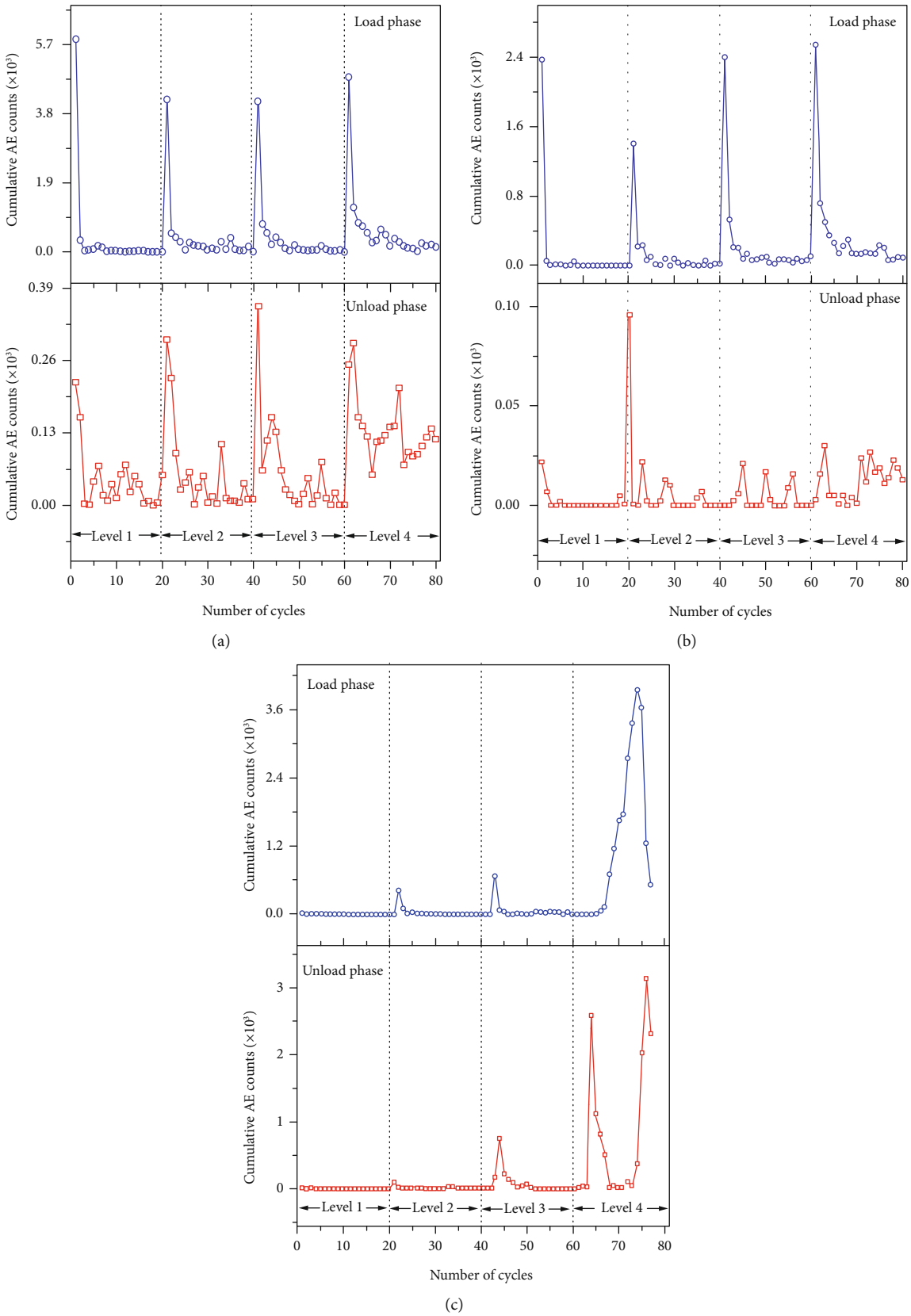

Figure 11: Evolution of cumulative AE events of coal versus cycles at different loading frequencies: (a) 0.1 Hz; (b) 0.2 Hz; (c) 0.5 Hz.

3.4. Acoustic Emission Characteristics of Coal Subjected to Different Frequencies under Multilevel Cyclic Loading. AE is defined as transient elastic waves produced by the release of elastic energy within materials [32, 33]. AE events are closely related to crack initiation, propagation, and coalescence of rock during the loading process [34]. Figure 10 shows the intensity of acoustic emission and loading stress versus time at different loading frequencies. Obviously, AE events intensified with the increase of peak stress amplitude. Also, the AE characteristics varied with the loading frequencies, especially at the frequency of 0.5 Hz. At the frequency 0.1 Hz and 0.2 Hz, the curve slope of cumulative AE energy or AE counts versus the loading time approximately kept constant at the first three peak stress amplitude levels ($0.2\sigma_c$-$0.6\sigma_c$). However, the AE events increased significantly at the peak stress amplitude of $0.8\sigma_c$, revealing that a large amount of new microcracks emerged. This indicates that fatigue damage of coal start at the early stage of cyclic loading at a low loading frequency. With further cyclic loading, significant damage can be accumulated in coal. This is the reason for the rapid increase trend of both cumulative AE counts and energy at the level IV in Figures 10(a) and 10(b). For the loading frequency of 0.5 Hz, the slope of cumulative AE counts and energy in terms of time levelled off at the first three levels. However, the slope of cumulative AE counts and AE energy in terms of time increased dramatically when the peak stress amplitude rose to $0.8\sigma_c$. This indicates that the damage time is delayed with the increase of loading frequency until the peak cyclic loading amplitude reaching a critical value.

Figure 11 shows the evolution of cumulative AE events of coal at different loading frequencies. It states that if a sample is subjected to a cyclic stress history, no acoustic emission occurs over a loading and unloading cycle until the applied stress exceeds the maximum of previously applied stress [35, 36]. At each stress level, the maximum AE counts occurred at the beginning of cyclic loading. After that, there are almost no AE counts during the rest cycles under the same level. However, when the loading frequency is 0.5 Hz, there are relatively few AE counts in the first three levels of peak cyclic stress amplitude ($0.2\sigma_c$-$0.6\sigma_c$), and the AE counts increased sharply at the peak stress amplitude of $0.8\sigma_c$. Meanwhile, it can be found that the Kaiser effect lags behind the loading stress. Figure 11 also shows that for the loading phase, the intensity of acoustic emission was higher than that of unloading phase. Compared to the loading phase, the distribution of acoustic emission fluctuated continuously during the unloading phase.

3.5. Evolution of Fatigue Damage. From the micro scale, the damage of coal under cyclic loading is a gradually progressive development process. The fatigue damage can be a growth of existing microcracks and development of new microcracks. Different from elastic deformation, this damage process is irreversible and usually tends to be nonlinear. Therefore, the degradation of rocks due to damage can make the loading modulus different from unloading modulus, which can be seen from Figure 4.

The wide pore-size distribution and cracks and fissures make fatigue damage of coaly rock complex. In order to investigate the evolution of fatigue damage in terms of number cycles, the load/unload response ratio (LURR) was used here [37]:

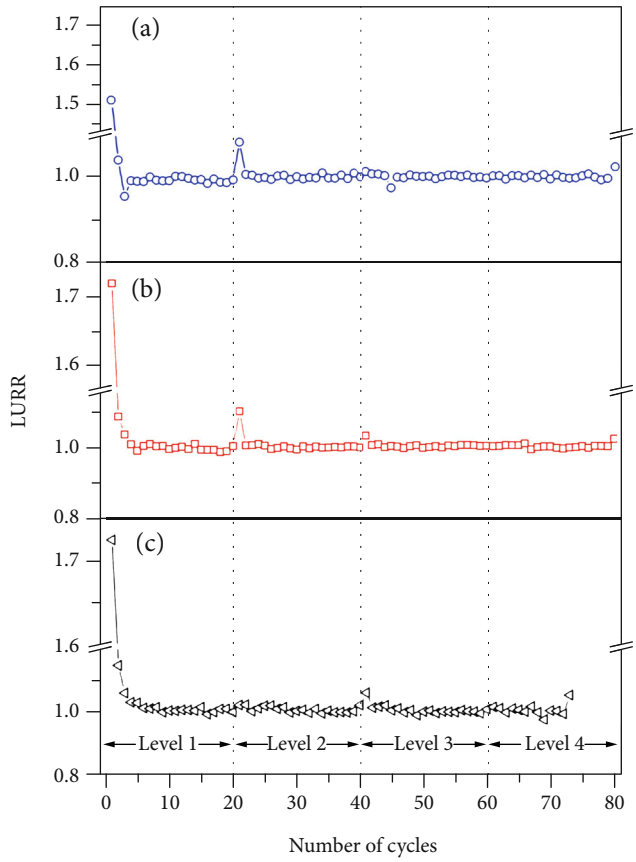

Figure 12: Evolution of LURR versus number of cycles at different loading frequencies: (a) 0.1 Hz; (b) 0.2 Hz; (c) 0.5 Hz.

$$Y = \frac{X_+}{X_-}, \tag{6}$$

where Y is the LURR and X stands for the response rate in loading/unloading process. The subscript "+" represents the loading process while "-" represents the unloading process. $Y = 1$ stands for the elastic deformation of coaly rock where $X_+ = X_-$, while $Y > 1$ for damage of coaly rock with $X_+ > X_-$. The more significant damage occurred in coaly rock, the larger Y will be. The LURR shows great priority in predicting the failure of complex system, such as earthquake and engineering material [38, 39].

The response rate X is defined as

$$X = \lim_{\Delta p \to 0} \frac{\Delta R}{\Delta P}, \tag{7}$$

where X is defined as the response rate, ΔP is the increment of P, and ΔR is the increment of R.

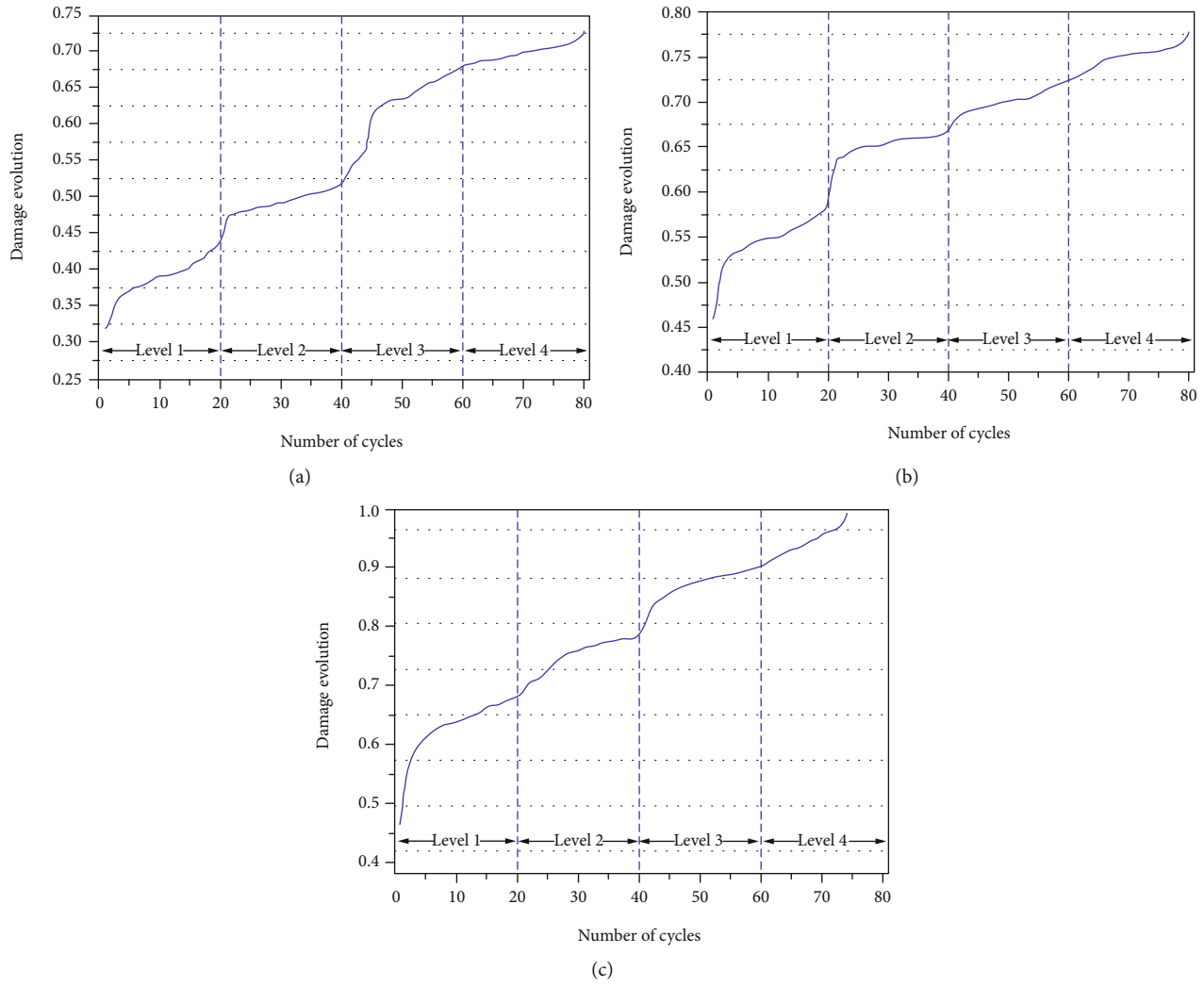

Figure 13: Evolution of cumulative damage versus number of cycles at different loading frequencies: (a) 0.1 Hz; (b) 0.2 Hz; (c) 0.5 Hz.

According to the constitutive relationship of linear elasticity, the X can be given as

$$X = \lim_{\Delta p \to \infty} \frac{\Delta R}{\Delta P} = \frac{\Delta \varepsilon}{\Delta \sigma} = \frac{1}{E}. \tag{8}$$

Substituting Eq. (7) into Eq. (6), the LURR can be expressed as

$$Y = \frac{X_+}{X_-} = \frac{1/E_+}{1/E_-} = \frac{E_-}{E_+}, \tag{9}$$

where E_+ and E_- refer to the elastic modulus under loading and unloading process, respectively.

The evolution of LURR in terms of number of cycles at different loading frequencies is illustrated in Figure 12. Figure 12 shows that LURR was initially larger than unity in the early stage of the first level of peak cyclic stress amplitude. This reason is that a large number of microcracks and voids were compacted, leading to the decrease in E_+ in the early stage of the first level of cyclic peak stress amplitude. With further cyclic loading, the coaly rock entered the linear elastic stage with $E_+ = E_-$. This indicates that the deformation mechanism of initial fissure or pore closure stage is different from the subsequent linear elastic stage. Mechanical damage

Table 1: Fitting results versus relative cycle at different loading frequencies under multilevel cyclic loading.

Frequency (Hz)	Stress level	M	N	R^2
0.1	1	0.01503	0.14274	0.96593
	2	3.49292E-5	0.07178	0.92323
	3	0.02891	0.35445	0.93863
	4	7.41856E-6	0.10895	0.85489
0.2	1	0.00435	0.16874	0.89212
	2	5.86179E-7	0.07824	0.98289
	3	1.48267E-5	0.11724	0.90325
	4	2.57051E-5	0.14168	0.92868
0.5	1	0.04693	0.4271	0.91539
	2	0.00738	0.33978	0.97632
	3	0.0071	0.50114	0.98981
	4	0.03939	1.26118	0.75365

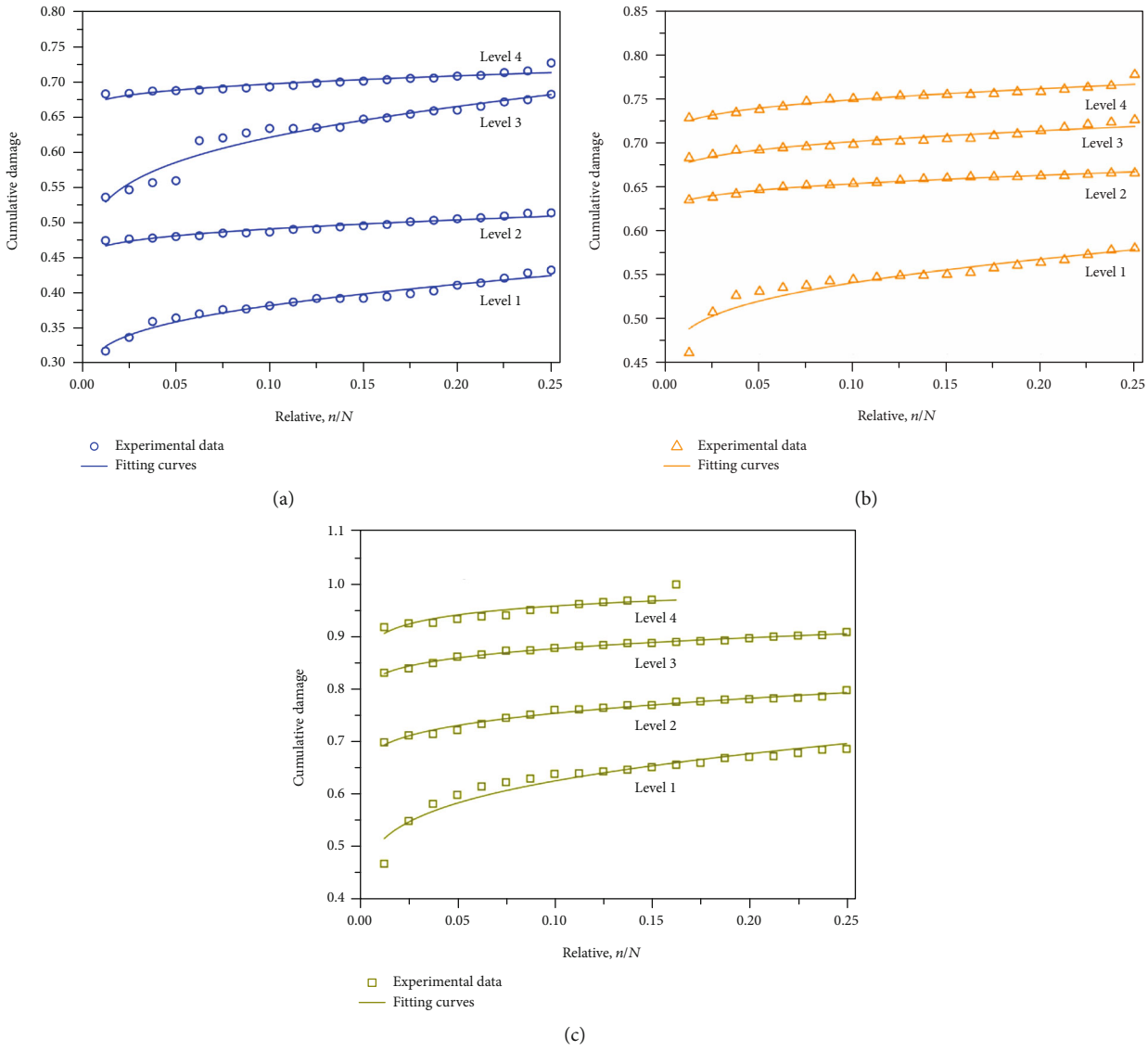

Figure 14: Comparison between the experimental values and fitting results versus relative cycle at different loading frequencies: (a) 0.1 Hz; (b) 0.2 Hz; (c) 0.5 Hz.

can be induced in the initial fissure or pore closure stage; however, no damage occurred in the linear elastic phase with Y approximately equal to unity.

Figure 12 also shows that LURR was greater than unity in the first or first several cyclic loading at both the loading frequency of 0.1 Hz and 0.2 Hz. However, such a phenomenon disappeared when the cyclic peak stress amplitude increased to level 3 ($0.6\sigma_c$) at 0.1 Hz and level 4 ($0.8\sigma_c$) at 0.2 Hz. Contrary to the loading frequency of 0.1 Hz and 0.2 Hz, the phenomena of LURR was greater than unity reappeared at the cyclic peak stress amplitude levels 3 ($0.6\sigma_c$) and 4 ($0.8\sigma_c$). This indicates that lower loading frequency of cyclic loading allows the damage to occur at the early time of cyclic loading and low peak cyclic stress amplitude. This is consistent with the findings from the AE response of coal as shown in Figure 10. Therefore, it can be concluded that LURR is an effective parameter to evaluate the damage of coaly rock under cyclic loading and also effective in distinguishing different deformation mechanism at different loading stages as mentioned above.

It has been known that a relation between LURR Y and damage variable D always exists, no matter the definition complexity or difference of damage variable D [40]. In order to further quantify the damage evolution of coaly rock under cyclic loading, a damage variable D is defined as below [41]:

$$D = 1 - \exp\left(\frac{1 - Y}{mY}\right), \tag{10}$$

where D is the damage variable and m is the Weibull index.

Figure 13 shows the evolution curve of cumulative damage of coal in terms of the number of cycles at different frequencies. Overall, the cumulative damage increased gradually with the number of cycles, following a nonlinear trend. The damage evolution not only reflects the whole

cyclic loading process, but also describes the damage of coal at the initial loading stage. Therefore, it is consistent with the progressive nature of coal during the whole loading process.

According to the linear multiaxis fatigue damage model proposed by Yin et al. [42], the cumulative damage of coal under cyclic loading at each stress level can be calculated [43]:

$$D = 1\text{-}\left\{1\text{-}\left(\frac{N_i}{N_t}\right)^{1/1-\alpha}\right\}^{1/1+\beta}, \quad (11)$$

where N_i is the number of cycles of the $i\ th$ level loading, N_t is the total number of cycles at the $i\ th$ stress level, α is the stress exponent, and β is the material constant related to the temperature.

Let $M = 1/(1-\alpha)$, $N = 1/(1+\beta)$; the fitting parameters of M and N under different loading frequencies are shown in Table 1. The data of accumulation damage of different stress levels under different loading frequencies is simulated with Eq. (11). The experimental results of coal samples and the predicted results with Eq. (11) are shown in Figure 14. It is obvious that the predicted results fit the experimental results very well. This implies that the accumulation damage model can effectively describe the damage evolution of coal under multilevel cyclic loading.

4. Conclusions

In order to evaluate and quantify the geotechnical property evolution of coal during resource extraction, the mechanical property and damage characterization of coal under different cyclic loading were experimentally investigated by conducting multilevel cyclic stress with different loading frequency. The loading/unloading response ratio (LURR) is used to evaluate the damage of coal under cyclic loading. The Young's modulus of coal initially increased sharply with a reducing increasing rate and then decreased with further loading-unloading cycles. Additionally, the increment in Young's modulus is largest at the lowest peak stress amplitude, and the absolute increment gradually decreased with the increase of peak stress amplitude. The Poisson's ratio of coal gradually increased at lower peak stress amplitudes and then increased sharply with the increase of peak stress amplitude until macro failure, following a stepwise rising trend. The transition of volumetric compressibility-dilatancy occurred earlier under a higher loading frequency. The dissipated energy density of coal overall increased with the increase of peak stress amplitude. In addition, the cumulative dissipated energy of coal presented an obvious three-stage trend.

It is also found that LURR is an effective parameter to evaluate the damage of coaly rock under cyclic loading and is also useful in distinguishing different deformation mechanism at different loading stage. The results also show that the damage of coal can initiate at the early stage of cyclic loading at a low loading frequency, and the increase in frequency of cyclic loading can delay the damage time, requiring a relatively higher level of peak cyclic stress amplitude. This was confirmed by both the AE monitoring and LURR analyses.

Data Availability

The data used to support the findings of this study are available from the corresponding author upon request.

Conflicts of Interest

The authors declare that there is no conflict of interest regarding the publication of this paper.

Acknowledgments

This study was financially supported by the Guizhou science and technology innovation talent support program project [Qianjiaohe KY (2019) 070]. The authors would like to thank Taoli coal mine for providing the coal blocks for specimen preparation.

References

[1] C. Cheng, X. Li, and H. Qian, "Anisotropic failure strength of shale with increasing confinement: behaviors, factors and mechanism," *Materials*, vol. 10, no. 11, 2017.

[2] C. Wang, S. Li, T. Zhang, and Z. You, "Experimental study on mechanical characteristics and fracture patterns of unfrozen/-freezing saturated coal and sandstone," *Materials*, vol. 12, no. 6, 2019.

[3] C. Piao, S. Lei, J. Yang, and L. Sang, "Experimental study on the movement and evolution of overburden strata under reamer-pillar coal mining based on distributed optical fiber monitoring," *Energies*, vol. 12, no. 1, 2019.

[4] J. Zhang and Y. Li, "Coal strength development with the increase of lateral confinement," *Energies*, vol. 12, no. 3, 2019.

[5] B. Cerfontaine and F. Collin, "Cyclic and fatigue behaviour of rock materials: review, interpretation and research perspectives," *Rock Mechanics and Rock Engineering*, vol. 51, no. 2, pp. 391–414, 2018.

[6] N. Gatelier, F. Pellet, and B. Loret, "Mechanical damage of an anisotropic porous rock in cyclic triaxial tests," *International Journal of Rock Mechanics and Mining Sciences*, vol. 39, no. 3, pp. 335–354, 2002.

[7] N. Erarslan, H. Alehossein, and D. J. Williams, "Tensile fracture strength of Brisbane tuff by static and cyclic loading tests," *Rock Mechanics and Rock Engineering*, vol. 47, no. 4, pp. 1135–1151, 2014.

[8] Q. B. Meng, M. W. Zhang, L. J. Han, H. Pu, and T. Y. Nie, "Effects of acoustic emission and energy evolution of rock specimens under the uniaxial cyclic loading and unloading compression," *Rock Mechanics and Rock Engineering*, vol. 49, no. 10, pp. 3873–3886, 2016.

[9] A. Taheri, N. Yfantidis, C. L. Olivares, B. J. Connelly, and T. J. Bastian, "Experimental study on degradation of mechanical properties of sandstone under different cyclic loadings," *Geotechnical Testing Journal*, vol. 39, no. 4, pp. 673–687, 2016.

[10] J. F. Liu, H. P. Xie, Z. M. Hou, C. H. Yang, and L. Chen, "Damage evolution of rock salt under cyclic loading in unixial tests," *Acta Geotechnica*, vol. 9, no. 1, pp. 153–160, 2014.

[11] A. Momeni, M. Karakus, G. R. Khanlari, and M. Heidari, "Effects of cyclic loading on the mechanical properties of a granite," *International Journal of Rock Mechanics and Mining Sciences*, vol. 77, pp. 89–96, 2015.

[12] H. Munoz and A. Taheri, "Local damage and progressive localisation in porous sandstone during cyclic loading," *Rock Mechanics and Rock Engineering*, vol. 50, no. 12, pp. 3253–3259, 2017.

[13] Y. J. Yang, H. Q. Duan, L. Y. Xing, S. Ning, and J. K. Lv, "Fatigue characteristics of limestone under triaxial compression with cyclic loading," *Advances in Civil Engineering*, vol. 2018, Article ID 8681529, 12 pages, 2018.

[14] Q. Huang, Y. He, and J. Cao, "Experimental investigation on crack development characteristics in shallow coal seam mining in China," *Energies*, vol. 12, no. 7, 2019.

[15] M. N. Bagde and V. Petroš, "Waveform effect on fatigue properties of intact sandstone in uniaxial cyclical loading," *Rock mechanics and rock engineering*, vol. 38, no. 3, pp. 169–196, 2005.

[16] J. Q. Xiao, D. X. Ding, G. Xu, and F. L. Jiang, "Inverted S-shaped model for nonlinear fatigue damage of rock," *International Journal of Rock Mechanics and Mining Sciences*, vol. 46, no. 3, pp. 643–648, 2009.

[17] D. Z. Song, E. Y. Wang, and J. Liu, "Relationship between EMR and dissipated energy of coal rock mass during cyclic loading process," *Safety Science*, vol. 50, no. 4, pp. 751–760, 2012.

[18] E. L. Liu, S. He, X. Xue, and J. Xu, "Dynamic properties of intact rock samples subjected to cyclic loading under confining pressure conditions," *Rock mechanics and rock engineering*, vol. 44, no. 5, pp. 629–634, 2011.

[19] L. J. Ma, X. Y. Liu, M. Y. Wang et al., "Experimental investigation of the mechanical properties of rock salt under triaxial cyclic loading," *International Journal of Rock Mechanics and Mining Sciences*, vol. 62, pp. 34–41, 2013.

[20] Z. C. Wang, S. C. Li, L. P. Qiao, and J. G. Zhao, "Fatigue behavior of granite subjected to cyclic loading under triaxial compression condition," *Rock Mechanics and Rock Engineering*, vol. 46, no. 6, pp. 1603–1615, 2013.

[21] S. Q. Yang, P. G. Ranjith, Y. H. Huang et al., "Experimental investigation on mechanical damage characteristics of sandstone under triaxial cyclic loading," *Geophysical Journal International*, vol. 201, no. 2, pp. 662–682, 2015.

[22] E. L. Liu and S. M. He, "Effects of cyclic dynamic loading on the mechanical properties of intact rock samples under confining pressure conditions," *Engineering Geology*, vol. 125, pp. 81–91, 2012.

[23] D. Y. Jiang, J. Y. Fan, J. Chen, L. Li, and Y. Cui, "A mechanism of fatigue in salt under discontinuous cycle loading," *International Journal of Rock Mechanics and Mining Sciences*, vol. 86, pp. 255–260, 2016.

[24] E. L. Liu, R. Q. Huang, and S. M. He, "Effects of frequency on the dynamic properties of intact rock samples subjected to cyclic loading under confining pressure conditions," *Rock Mechanics and Rock Engineering*, vol. 45, no. 1, pp. 89–102, 2012.

[25] J. Q. Xiao, D. X. Ding, F. L. Jiang, and G. Xu, "Fatigue damage variable and evolution of rock subjected to cyclic loading," *International Journal of Rock Mechanics and Mining Sciences*, vol. 47, no. 3, pp. 461–468, 2010.

[26] J. Y. Fan, J. Chen, D. Y. Jiang, S. Ren, and J. X. Wu, "Fatigue properties of rock salt subjected to interval cyclic pressure," *International Journal of Fatigue*, vol. 90, pp. 109–115, 2016.

[27] K. Fuenkajorn and D. Phueakphum, "Effects of cyclic loading on mechanical properties of Maha Sarakham salt," *Engineering Geology*, vol. 112, no. 1-4, pp. 43–52, 2010.

[28] C. B. Jiang, M. K. Duan, G. Z. Yin et al., "Experimental study on seepage properties, AE characteristics and energy dissipation of coal under tiered cyclic loading," *Engineering Geology*, vol. 221, pp. 114–123, 2017.

[29] B. Sun, Z. D. Zhu, C. Shi, and Z. H. Luo, "Dynamic mechanical behavior and fatigue damage evolution of sandstone under cyclic loading," *International Journal of Rock Mechanics and Mining Sciences*, vol. 94, pp. 82–89, 2017.

[30] C. J. Jia, W. Y. Xu, R. B. Wang, W. Wang, J. C. Zhang, and J. Yu, "Characterization of the deformation behavior of fine-grained sandstone by triaxial cyclic loading," *Construction and Building Materials*, vol. 162, pp. 113–123, 2018.

[31] C. E. Fairhurst and J. A. Hudson, "Draft ISRM suggested method for the complete stress-strain curve for intact rock in uniaxial compression," *International Journal of Rock Mechanics and Mining Science and Geomechanics Abstracts*, vol. 36, no. 3, pp. 281–289, 1999.

[32] G. Royer-Carfagni and W. Salvatore, "The characterization of marble by cyclic compression loading: experimental results," *Mechanics of Cohesive-frictional Materials*, vol. 5, no. 7, pp. 535–563, 2000.

[33] R. D. Peng, Y. Ju, J. G. Wang, H. P. Xie, F. Gao, and L. T. Mao, "Energy dissipation and release during coal failure under conventional triaxial compression," *Rock Mechanics and Rock Engineering*, vol. 48, no. 2, pp. 509–526, 2015.

[34] D. A. Lockner, J. D. Byerlee, V. Kuksenko, A. Ponomarev, and A. Sidorin, "Chapter 1 observations of quasistatic fault growth from acoustic emissions," *International Geophysics*, vol. 51, pp. 3–31, 1992.

[35] P. Antonaci, P. Bocca, and D. Masera, "Fatigue crack propagation monitoring by acoustic emission signal analysis," *Key Engineering Materials*, vol. 465, pp. 370–373, 2011.

[36] H. P. Xie, J. F. Liu, Y. Ju, J. Li, and L. Z. Xie, "Fractal property of spatial distribution of acoustic emissions during the failure process of bedded rock salt," *International Journal of Rock Mechanics and Mining Sciences*, vol. 48, no. 8, pp. 1344–1351, 2011.

[37] J. Kaiser, *An Investigation into the Occurrence of Noises in Tensile Tests, or a Study of Acoustic Phenomena in Tensile Tests [Ph.D. Thesis]*, Tech Hosch Munchen Munich, Germany, 1950.

[38] A. Lavrov, "Kaiser effect observation in brittle rock cyclically loaded with different loading rates," *Mechanics of Materials*, vol. 33, no. 11, pp. 669–677, 2001.

[39] X. C. Yin, L. P. Zhang, H. H. Zhang et al., "LURR's twenty years and its perspective," *Pure and Applied Geophysics*, vol. 163, no. 11-12, pp. 2317–2341, 2006.

[40] X. C. Yin, X. Z. Chen, and Z. P. Song, "The development of load-unload response ratio theory and its application to earthquake prediction," *Chinese Journal of Geophysics*, vol. 37, no. 1, pp. 223–230, 1994.

[41] Y. X. Zhao, S. Gong, T. Teng, Y. D. Jiang, Z. L. Yang, and K. Chen, "Characterization of the load/unload response ratio for raw coal under uniaxial multi-level cyclic loading," *Chinese Journal of Rock Mechanics and Engineering*, vol. 37, no. 5, pp. 1096–1105, 2018.

[42] X. C. Yin, Y. C. Wang, K. Y. Peng, Y. L. Bai, H. T. Wang, and X. E. Yin, "Development of a new approach to earthquake

prediction: load/unload response ratio (LURR) theory," *Pure and Applied Geophysics*, vol. 157, no. 11, pp. 2365–2383, 2000.

[43] L. P. Zhang, H. Z. Yu, and X. C. Yin, "Failure potential evaluation in engineering experiments using load/unload response ratio method," *Pure and Applied Geophysics*, vol. 170, no. 1-2, pp. 237–245, 2013.